Biomechanics and Modeling in Mechanobiology
https://doi.org/10.1007/s10237-017-0988-1

ORIGINAL PAPER

Estimates for the acoustical stimulation and heating of multiphase biotissue

T. I. Zohdi[1] · **R. Krone**[1]

Received: 5 June 2017 / Accepted: 14 November 2017

Abstract
Low-intensity, unfocused, ultrasound-induced diathermy can produce undesired temperature increases at the interface of adjacent tissues within the body; particularly, at the interface of soft tissue and bone. This study provides a computational framework for predicting an upper bound on the temperature profile within a multiphase system composed of gel pad (water), tissue and bone from an input of acoustic energy, at frequencies and power levels consistent with applications of therapeutic hyperthermia. The model consists of solving a (one-dimensional) spatially discretized bioheat transfer equation via finite-difference method and updating the solution in time with a forward-Euler scheme. Simulations are then compared to experimental data to determine the energy-to-heat conversion factors within each constituent material using thermocouple-embedded, tissue-mimicking phantom material, with and without bone. Viscous heating artifacts from the presence of the thermocouples in the experimental phantom tissue are accounted for via additional experimental methods similar to those described by Morris et al. (Phys Med Biol 53:4759, 2008). Finally, an example application of the model is presented via prediction of the maximum temperature at the tissue–bone interface, as well as the peak temperatures in the composite structure at the end of a prescribed 2-min sonication, of blood-perfused, human soft-tissue at 1, 2 and 3 MHz frequencies and a spatial peak temporally averaged intensity of 1.0 W/cm^2. The results of this simulation are then related to comparable experimental studies in the literature.

Keywords Acoustics · Preferential heating · Unfocused ultrasound · Hyperthermia · Diathermy

1 Introduction

Applications of focused ultrasound for hyperthermic purposes, particularly ablation via thermal damage (i.e. 75–90 °C, per Rhoon and Gerard 2013), where highly localized temperature changes are intended and expected, the use of *unfocused* ultrasound for more mild diathermy (i.e. 40–45 °C, per Nyborg 2001; Dewhirst et al. 2005), typical in physiotherapy and applications for which cell necrosis is undesired, doesn't inherently raise concerns of localized, preferential and unexpected tissue heating. However, as has been repeatedly shown in studies (e.g. Corry et al. 1982; Fessenden et al. 1984; Hynynen and DeYoung 1988; Hynynen 1990; Lehmann et al. 1967; Lehmann et al. 1966; Marmor et al. 1979; Nelson et al. 1950; Smith et al. 2001), diathermy from unfocused, low-intensity ultrasound can result in preferential heating and potential tissue damage, at the interface of adjacent tissues within the body; particularly those of soft-tissue and bone. Typically, to avoid this undesired regional heating in sub-surface structures, clinical practitioners recommend using Pulsed Wave (PW) instead of Continuous Wave (CW) ultrasound, as well as either movement of the transducer itself on the application site (Hill et al. 2004; Bellew et al. 2016) or scanning the beam through the treatment volume (Shimm et al. 1988). PW ultrasound mitigates potential standing (convergent) ultrasound waves within the tissue (from normal reflections at tissue interfaces) and moving the transducer effectively averages (temporally) the acoustic energy absorbed per unit tissue area in the beam cross section. However, as applications of *stationary* transducers (unmoved and non-scanning) are becoming more prevalent in applications of low-level diathermy, preferential heating can posit a much greater threat; as such, is investigated here.

✉ T. I. Zohdi
zohdi@me.berkeley.edu

[1] Department of Mechanical Engineering, University of California, 6195 Etcheverry Hall, Berkeley, CA 94720-1740, USA

Published online: 22 November 2017

Unfocused ultrasound is typically modeled as a series of longitudinal plane waves which pass through all tissues within the beam profile, along the direction of wave propagation and attenuate as longitudinal and transverse waves in the medium (Hill et al. 2004; Morris et al. 2008). The energy of the waves dissipate with distance (i.e., tissue depth) via molecular friction (and subsequent heating), as well as loss to the surroundings from mechanical work. Spatial attenuation is typically modeled as a decreasing exponential with tissue depth (Hill et al. 2004; Nyborg 2001). However, as the waves encounter regions with large differences in acoustic impedance (e.g., from soft tissue to bone), reflections, absorption and scattering occur which give rise to regional spikes in energy deposition, subsequent heating and additional loss (Mayer 1965). Additionally, it has been shown that absorption increases as the angle of incidence to the interface plane becomes more normal (Chan et al. 1973; Lin et al. 2000). Therefore, predicting undesired temperature increases at the tissue–bone interface has been a major challenge in applications of low-intensity, unfocused, stationary ultrasonic diathermy.

Chan et al. (1973, 1974) used an analytical approach to highlight the importance of the incident beam angle from plane waves on the amount and location of heating in a model of fat–muscle–bone where Lin et al. (2000) has studied the absorbed power deposition across a muscle–cortical–spongy bone interface. Further, although focused ultrasound hyperthermia was used in Fujii et al. (1999), the importance of the muscle–bone interface to preferential heat generation was both theorized and experimentally validated with phantom-implanted thermocouples.

We examine by simplified, one-dimensional computational methods, the conditions under which worst-case heating can occur at a tissue–bone interface, given a stationary input of ultrasound energy at an intensity (power per unit area) and for a range of frequencies common for low-level hyperthermia (Draper et al. 1995). The incident ultrasound beam is considered normal to the surface of each material interface, for maximum energy absorption. Further, an idealized composite structure is considered as being a narrow, unit-area cross section in a single dimension (i.e., ignoring heat radial heat conduction as a conservative case) with material lengths corresponding to thicknesses of the following: acoustic standoff (water; gel pad), tissue anterior to bone, bone and finally tissue posterior to the bone (Fig. 1). The convective heat loss from blood perfusion is also considered in the model. Lastly, we assume a numerical scaling factor which adjusts for both the energy converted into heat in each material section as well as that which is lost to radial conduction. These scaling factors are then determined, experimentally. Finally, a sample simulation is run and compared to results from literature.

2 Background

For simulating the time-dependent thermodynamic response of biological tissue to ultrasonic heating, the rise in temperature at any point in the material is governed by the familiar bioheat equation from Pennes (1948) as,

$$\rho C \frac{\partial T}{\partial t} = k\nabla^2 T + \dot{Q} - \omega_b C_b \left(T - T_b\right). \tag{1}$$

This is an energy balance of conductive losses in the tissue ($k\nabla^2 T$), the convective loss through blood perfusion ($\omega_b C_b \left(T - T_b\right)$) and an internal heat source term ($\dot{Q}$); all in units of power per unit material volume, where ρ is the density $[Kg/m^3]$, C is the specific heat capacity $[J/Kg*K]$, k is the thermal conductivity $[W/m*K]$, ω_b is the blood perfusion constant $[Kg/m^3*s]$, C_b is the specific heat capacity of blood and T_b is the circulating blood temperature $[K]$. We can simplify for one dimension and note the material properties change as a function of depth (e.g., $k(x)$) in a multi-material structure. Additionally, all materials are assumed isotropic in their thermomechanical response to perturbations. We assume here that not all acoustical energy input to the system is converted into heat (i.e., some is lost to mechanical work to the surroundings and doesn't manifest as a heat source, $\dot{Q}$), so a tunable scaling factor θ is introduced representing the percentage of energy from an ultrasound wave that gets absorbed as heat traveling through a composite medium, where $0 \leq \theta \leq 1$ ($\theta = 1$ corresponds to 100% conversion to heat). Note that since the simulation is only one dimensional, radial heat loss to the surroundings is neglected; however, a reasonable assumption can be made that accounting for this radial loss can be accomplished by θ as well (i.e., θ represents scales the heating to account for both the radial heat loss as well as the percentage of energy conversion). Further, note that θ is different for each tissue (e.g., tissue and bone; although, isotropic w.r.t. each material) as energy conversion into heat via molecular friction is different for distinct material compositions. Only longitudinal waves (and not transverse or shearing waves) are considered here as adding to the heat generation within a material layer (Haken et al. 1992). Combining these assumptions, we have,

$$\rho C \frac{\partial T}{\partial t} = \frac{\partial}{\partial x}\left(k \frac{\partial T}{\partial x}\right) + \theta \dot{Q} - \omega_b C_b \left(T - T_b\right). \tag{2}$$

The rate of energy input to the system from the attenuation of ultrasonic energy is commonly represented (Hill et al. 2004; Nyborg 1988) as the exponential decay as a function of material depth (x),

$$\dot{Q} = \alpha I e^{(-\alpha x)}, \tag{3}$$

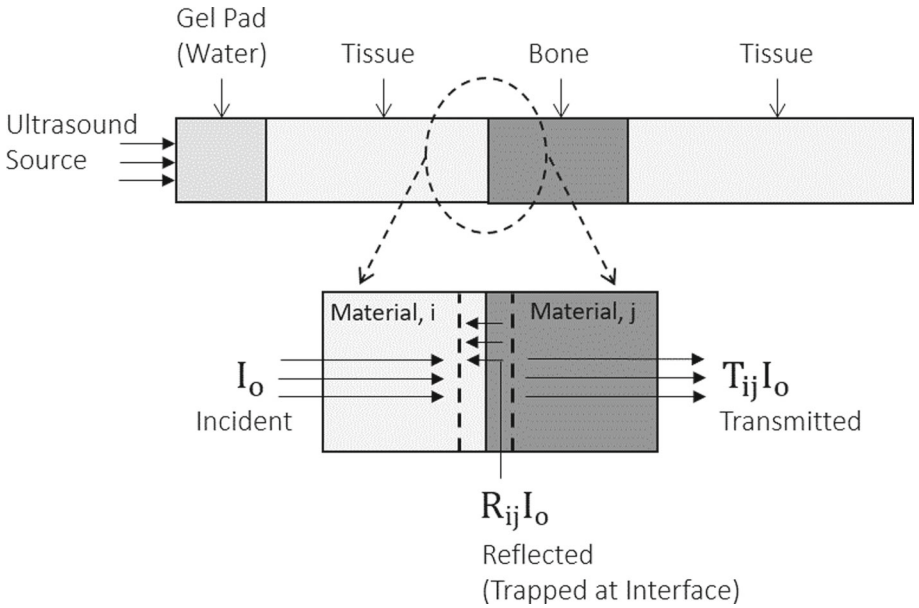

Fig. 1 1D composite structure of gel pad (water), tissue, bone and tissue. Normal-incident intensity (I_o, power per unit cross-sectional material area) is shown scaled by reflection ($R_{ij}\,I_o$) and transmission ($T_{ij}\,I_o$) at the material interfaces. All reflected intensity is numerically considered 'trapped' at the interface computational points (nodes) for conservative estimates of peak preferential heating

where, α is the attenuation coefficient of the material (assuming the attenuation and absorption coefficients are equal and all attenuated, i.e., absorbed, energy results in heating the tissue) and I is the acoustic, spatially-averaged, temporal peak intensity $[W/m^2]$. Further, the rate of energy transmitted (positive x-direction) through the composite layers and reflected (negative x-direction) from the material interfaces is handled by the same expression.

In general, two adjacent materials (i and j, where $i = 1,\ldots,N-1$ and $j = 2,\ldots,N$ and where N is the total number of distinct material layers in the composite) with acoustic impedance (Z_i and Z_j, respectively) where $Z \equiv \rho c$ and c is the sound speed in the material [m/s], the *maximum* percentage of *normal* incident energy (or power) transmitted through the material interface (from i to j—see Fig. 1) is governed by the dimensionless ratio,

$$T_{ij} = \frac{2Z_j/Z_i}{\left(Z_j/Z_i + 1\right)}. \tag{4}$$

Similarly, the amount of normal-incident energy (or power) reflected from the interface (i.e., from j to i) is given by,

$$R_{ij} = \frac{\left(Z_j/Z_i - 1\right)}{\left(Z_j/Z_i + 1\right)}. \tag{5}$$

where of course energy conservation at the interface further requires $R_{ij} + Tij = 1$. A brief inspection of these ratios illustrates that waves traveling from a low-density material (e.g., tissue) to a high one (e.g., bone) are mostly reflected at the material interface. Hence, normal-incident waves constructively interfere near the interface, producing spikes in the ultrasound pressure field and subsequent local heating. Waves that do transmit through the interface into the higher density material may produce additional excess heating near the interface, depending on the absorption coefficient of the material (Marmor et al. 1979).

3 Numerical methods

For the purposes of investigating worst-case (upper bound) preferential heating of the tissue–bone interface, the reflected energy is (computationally) assumed to remain trapped at the interface (i.e., within a single discretization length, Δx and added numerically to the computational node nearest the interface). Additionally, we assume no phase difference between reflected and transmitted waves between materials (hence, maximum constructive wave interference). Therefore, in each section of the multiphase material, there are two contributors at steady state to the heat generation, namely energy transmitted into a material layer and energy reflected from the interface with the material layer following it.

Considering first only the conduction term of (2), we can approximate the partial spatial derivative according to the following discretization scheme,

$$\begin{aligned}\frac{\partial}{\partial x}\left(k(x)\frac{\partial T(x,t)}{\partial x}\right) &\approx \frac{1}{\Delta x^2}\left\{k\left(x+\frac{\Delta x}{2}\right)\left[T(x+\Delta x)-T(x)\right]\right.\\ &\left.-k\left(x-\frac{\Delta x}{2}\right)\left[T(x)-T(x-\Delta x)\right]\right\}\end{aligned} \tag{6}$$

Table 1 Material properties and thicknesses

Parameter	Symbol	Water	TMM	Soft tissue	Bone	Blood	Units
Density	ρ	993[c]	1030[b]	1041[c]	1990[c]	–	Kg/m^3
Sound speed	c	1540[c]	1561[b]	1580[c]	3359[c]	–	m/s
Thermal conductivity	k	0.60[a]	0.58[b]	0.44[a]	0.29[a]	–	$W/m*K$
Specific heat	C	4178[c]	3660[b]	3360[a]	1300[c]	3840[c]	$J/Kg*K$
Attenuation Coefficient (1 MHz)	α	0.0002[a]	0.0736[b]	0.17[a]	2.5[c]	–	Np/cm
Perfusion Constant	ω_b	–	–	2.0[d]	0.0	–	Kg/m^3*s
Thickness	Δx	1.2	2.0	2.0	2.5	–	cm

[a] Hill et al. (2004)
[b] King et al. (2011)
[c] Duck (2013)
[d] Lin et al. (2000)

To simplify the notation, we define the following,

$$A(x,t) \equiv \frac{1}{\Delta x^2}\left\{k\left(x+\frac{\Delta x}{2}\right)\left[T(x+\Delta x)-T(x)\right] - k\left(x-\frac{\Delta x}{2}\right)\left[T(x)-T(x-\Delta x)\right]\right\} \tag{7}$$

where the spatial (one-dimensional) domain is split into equal segments (Δx) between nodes, $i = 1, 2, \ldots, N$, where the field quantities (e.g., temperature) are calculated. This finite-difference method allows for simple numerical solutions of the partial differential equation (2) by first approximating the spatial derivatives at each node at a given time step, calculating the temperature, then advancing a time step (of duration Δt) and updating the spatial solutions. Since we cannot calculate the quantity $k\left(x+\frac{\Delta x}{2}\right)$, which refers to the value of the thermal conductivity of the material located between two nodes (i.e., at $x+\frac{\Delta x}{2}$, which is unknown), we can further approximate these quantities with,

$$k\left(x+\frac{\Delta x}{2}\right) \approx \frac{1}{2}\left(k(x)+k(x+\Delta x)\right), \tag{8}$$

and,

$$k\left(x-\frac{\Delta x}{2}\right) \approx \frac{1}{2}\left(k(x)+k(x-\Delta x)\right). \tag{9}$$

Finally, we use a forward-Euler temporal discretization in which we approximate the time derivative with,

$$\frac{\partial T(x,t)}{\partial t} \approx \frac{T(x,t+\Delta t)-T(x,t)}{\Delta t}. \tag{10}$$

Therefore, using (2) and (6, 7) with (10), we have the following updating scheme for each node (i) in the system (excluding the boundary nodes, which are assumed fixed in time at T_o),

$$T(x_i,t+\Delta t) = \frac{\Delta t}{\rho_i C_i}\left[A(x_i,t)+\theta_i\dot{Q}_i-\omega_b C_b\left(T(x_i,t)-T_b\right)\right] + T(x_i,t), \tag{11}$$

where the material constants vary with depth in the composite, i.e., $\rho_i \equiv \rho(x_i)$, $C_i \equiv C(x_i)$ and $\alpha_i \equiv \alpha(x_i)$.

Additionally, for the first material layer (i.e., $i = 1$), the heat generated in the layer by the attenuation of ultrasonic energy (as a function of depth in material, x_1) is, $\dot{Q}_1(x_1) = \alpha_1 I_o e^{(-\alpha_1 x_1)}$, where $I_o = I(x_1 = 0)$ is the incident ultrasound intensity (in W/m^2) at $x_1 = 0$.

Similarly, for each subsequent middle material layer (i.e., excluding the last material, so for $i = 2, \ldots, N-1$), the total heating in the material is the sum of the contributions from power transmitted from the previous material and that which is reflected from the interface of the subsequent material. For the last material (i.e., $i = N$), we assume an infinite boundary condition where there is no reflection at the boundary. Therefore, the only heating input to this layer comes from the attenuation of the power transmitted through the interface from the previous material (i.e., $i = N-1$).

The spatial and temporal discretization parameters chosen for all simulations are $\Delta x = 0.49751$ mm and $\Delta t = 0.0001$ seconds. Δx corresponds to segmenting the spatial domain of 10 cm with a numerical mesh density of 201 nodes. This mesh density was adopted in accordance with Shimm et al. (1988) who points out that wavelengths in soft tissue of ultrasound at clinically relevant frequencies (e.g. near 1 MHz) are a millimeter or less. Only when the dimensions of the volume to be heated are similar to the wavelength, can power be maximally absorbed. Lastly, additional mesh refinements studied here showed $< 1\%$ changes in results.

Table 1 summarizes the material constants used in numerical simulations.

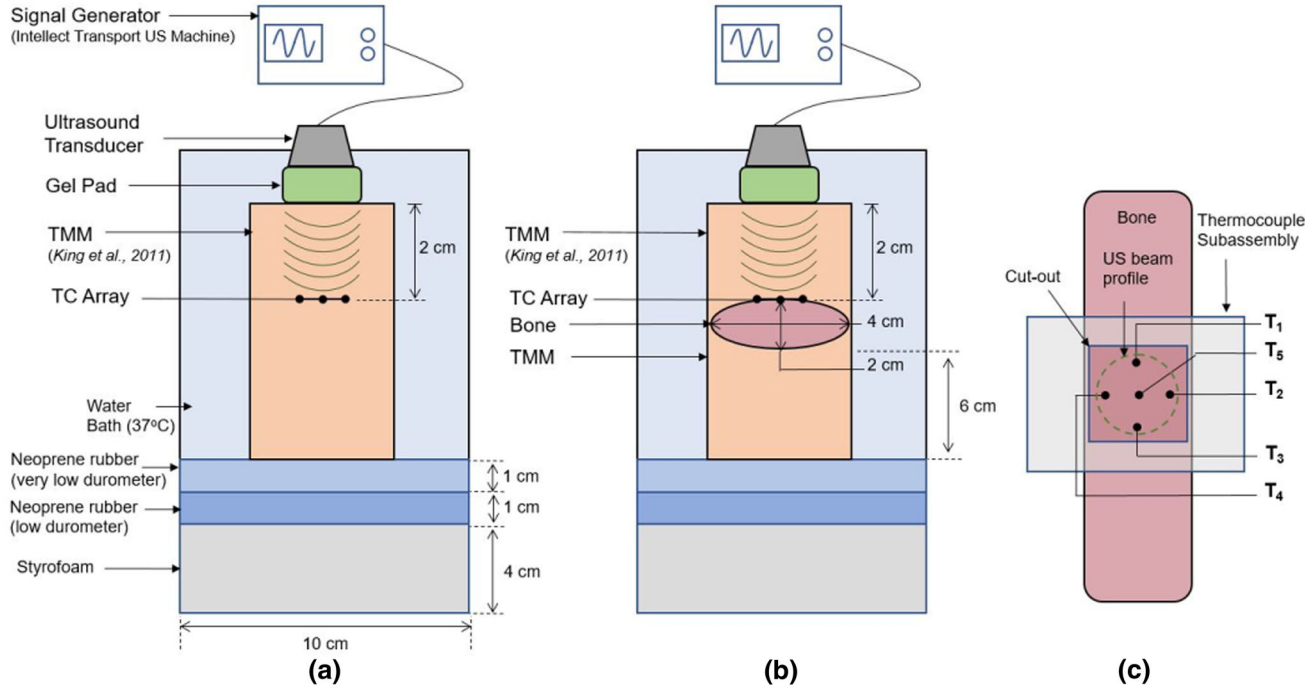

Fig. 2 Experimental setup showing (**a**) TMM-only phantom with thermocouples suspended at a known axial distance from the ultrasound transducer and immersed in a 37^{o}C water bath, (**b**) TMM–bone–TMM phantom, comprised of two pre-cast TMM sections above and below a fresh, degassed bovine rib bone with the thermocouple subassembly on the surface of the bone, immersed in a 37 °C water bath and (**c**) top view of the bone and thermocouple subassembly composed of a thin polycarbonate sheet with thermocouples affixed and suspended over a center cutout portion

4 Experimental methods and materials

In order to conduct numerical simulations of the tissue–bone heating from the input of acoustic energy (i.e., to solve Eqn. 11), the numerical scaling factors, θ_i, in (11) for the tissue and bone, first had to be experimentally determined (water was assumed an arbitrarily small value).

As such, to approximate θ_i for human soft-tissue (i.e., the numerical scaling of energy converted into heat and lost radially in the tissue, hence not accounted for in the 1D simulation), ultrasound experiments with embedded thermocouples on a *phantom* tissue-mimicking material (TMM) were formulated per specifications described in King et al. (2011) were conducted. Numerical simulations of only TMM (with appropriate material constants per King et al. 2011) were then conducted where θ_i was adjusted until the numerical temperature predicted at the experimental thermocouple depth in the TMM matched experimental temperatures recorded over time. After establishing θ_{TMM}, a similar experiment and simulations were conducted with the inclusion of a fresh, degassed bovine rib bone, with thermocouples attached to the surface, suspended at a known depth within the TMM. This then established θ_{Bone}. Finally, a last experiment was conducted to isolate the viscous heating artifact from the presence of the thermocouples themselves which was then subtracted from all measured experimental temperature values following Morris et al. (2008). Details for these experiments are described below.

4.1 Determining θ_{TMM} and θ_{Bone}

4.1.1 Experiments and simulations on a TMM-only phantom

TMM was formulated per specifications in King et al. (2011) and cast (at 70 °C) into a prescribed container (approximately 5 cm × 10 cm × 10 cm) over a pre-assembled thermocouple (TC) subassembly, which was itself suspended at a 2 cm depth under the top surface of the TMM (Fig. 2a). The TC subassembly consists of an array of five fine-wire thermocouples (Omega fine-wire, T-Type, 125 micron, copper-constantan) attached via transparent tape in a circular pattern onto a thin (0.50 mm) sheet of polycarbonate containing a 3 cm × 3 cm cutout to prevent occlusion of the passing ultrasound beam (Fig. 2c). This TMM-only phantom (with embedded TC array) was then immersed in a 37 °C water bath to provide a stable equilibrium temperature and acoustic coupling between the gel pad, TMM and ultrasound transducer. Additionally, the TMM phantom was stacked on layers of soft neoprene rubber and styrofoam to prevent far-field reflections. Following thermal equilibrium

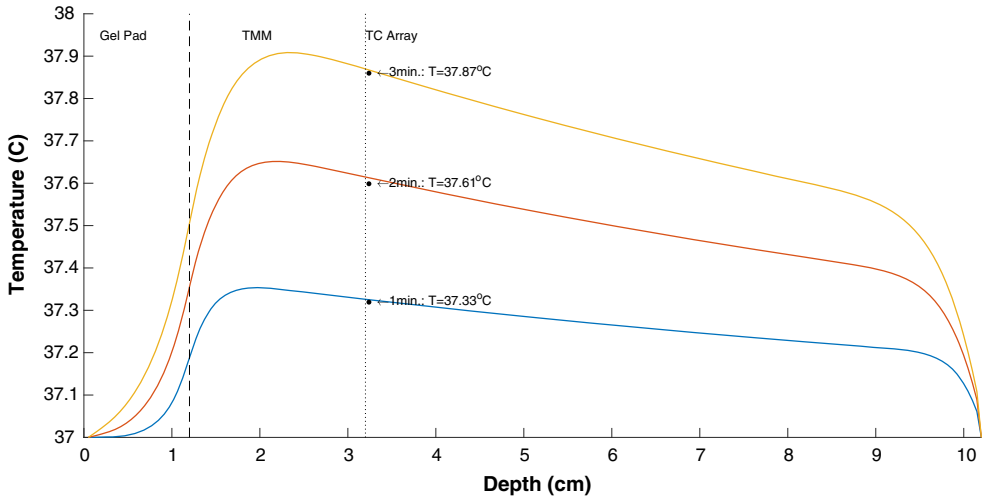

Fig. 3 Simulation of TMM-only showing temperature as a function of material depth with temperature at the location of the experimental TC array highlighted, from several minutes of 1 MHz sonications of 0.5 W/cm^2

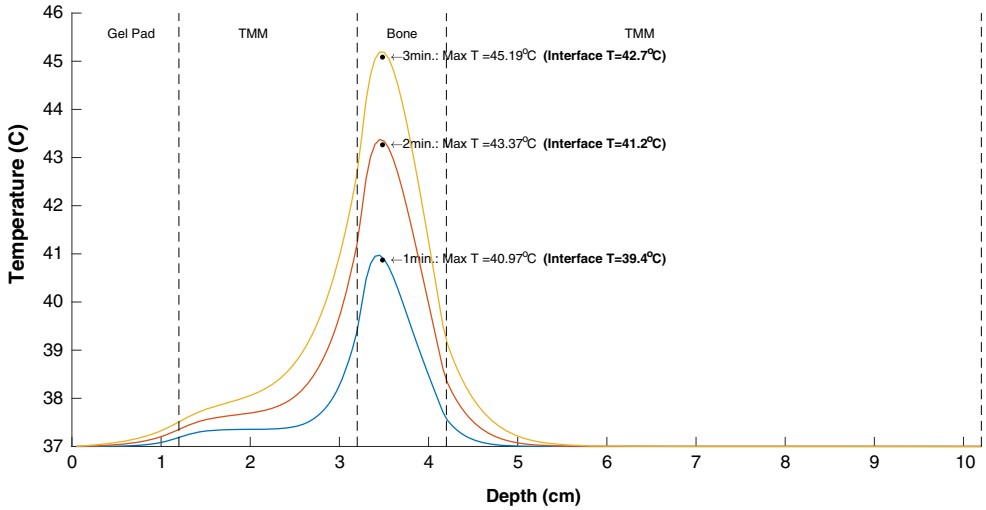

Fig. 4 Simulation of TMM-bone showing temperature as a function of material depth for sonication times of 1, 2 and 3 min at 1 MHz and 0.5 W/cm^2. The TMM-bone interface and maximum temperatures are highlighted

of the TMM phantom, PW ultrasound sonications of several minutes were conducted at 0.5 W/cm^2, where the peak (center) temperature in the TC array was recorded (Fig. 3, PicoTech DAQ, TC-08 at a sampling rate of 0.200 seconds). Numerical simulations were conducted until the predicted temperature at a 2 cm depth in the TMM matched experimental values (peak TC value, averaged over six experiments) to within 1%. This determined that value for θ_{TMM} as 0.685, or 68.5% of the energy is converted into heat within the TMM and the remainder lost to radial conduction and mechanical work. We assume in subsequent simulations on soft tissue–bone interface heating that $\theta_{TMM} = \theta_{Tissue}$.

4.1.2 Experiments and simulations on a tissue–bone phantom

Similar to the TMM-only phantom, TMM was again formulated per King et al. (2011) and cast over a fresh bovine rib bone (approximately 1 cm × 3 cm × 10 cm), previously degassed in pH-buffered saline solution for 1 hour, with the TC subassembly placed onto the surface of the degassed bone so each TC junction was directly in contact with the periosteum of the bone. The TC subassembly was again kept at a depth of 2 cm below the top surface of the TMM and the entire phantom assembly measured approximately 5 cm × 10 cm and 6 cm thick. Again, the TMM–bone phantom was stacked on layers of soft neoprene rubber and

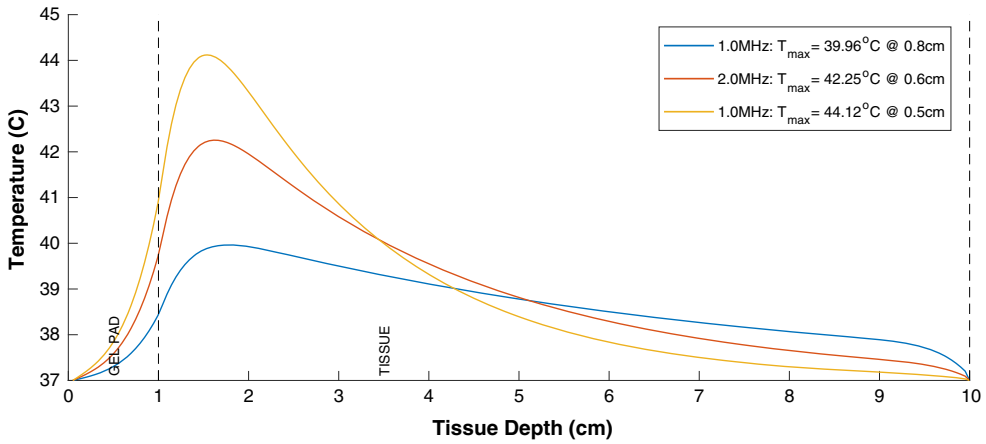

Fig. 5 Simulations showing the stationary, unfocused ultrasound heating in human soft tissue at the end of a 2-min sonication of I_{SPTA} = 1.0 W/cm^2 at various frequencies. The maximum tissue temperature is shown along with the depth beyond the interface of gel pad and tissue at which it occurs

styrofoam to prevent far-field reflections (Fig. 2b). Following thermal equilibrium of the TMM–bone phantom, PW ultrasound sonications of several minutes were conducted at 0.5 W/cm^2, where the peak (center) temperature in the TC array was recorded. Numerical simulations were run until the predicted temperature at the TMM–bone interface matched experimental values (peak TC value, averaged over six experiments) to within 1%. This determined that value for θ_{Bone} (θ_{TMM} being previously set) as 0.662, or 66.2% of the energy is converted into heat within the bone and the remainder lost to radial conduction and mechanical work (Fig. 4).

4.2 Viscous heating from thermocouples

The use of thermocouples in experiments involving ultrasound sonication has been shown (see Morris et al. 2008) to add a thermal artifact. This measured, aberrant thermal increase is due to the relative molecular motion of the semiliquid media surrounding the motionless solid of the thermocouple junction, caused by the ultrasound waves. This experimental artifact can be itself determined via methods such as that described in Morris et al. (2008), which we emulate in this study. Following Morris, we conduct a separate experiment where a thermocouple is suspended (i.e., cast) into a low-attenuation (i.e., absorbing) material and the transient temperature is measured over a short period of time during ultrasound sonication. To this end, we suspended a single 0.125 mm, T-type insulated fine-wire thermocouple in multiple 2 cm thick sections of Aquaflex gel pads (Parker Laboratories), which were themselves placed into a degassed waterbath maintained at 37°C to acoustically couple between the sections. Under this stack are multiple layers of (0.50 cm thick) soft neoprene rubber to attenuate far-field ultrasound reflections. To the top surface of the Aquaflex gel pad, the an ultrasound transducer is placed in direct contact with the water in the bath as the coupling media. Targeting the thermocouple in the cross section of the ultrasound beam was accomplished by measuring the temperature and moving the transducer perpendicular to the beam axis in small ($\leq$ 1 mm) steps until a maximum temperature is found. Finally, the change in temperature after multiple, 1 MHz, 2.0 W, 50-second sonications (with 50 seconds of off-time, between) was measured and then averaged to determine the thermal artifact of approximately 1 °C; corresponding to 5% of the measured temperature. Therefore, in matching simulations to experimental results, 1 °C was subtracted from all experimentally measured temperature values.

5 Results

To illustrate a simulation on the preferential heating of the *tissue*–bone interface, we use experimentally determined θ_{Bone} and assumed $\theta_{TMM} = \theta_{Tissue}$, while applying material parameters for soft-tissue from Table 1 to the model. We choose a nominal value of spatial average temporal peak intensity of 1.0 W/cm^2 and show a range of frequencies of 1, 2 and 3 MHz. Figure 5 shows the evolution of the temperature with tissue depth, as an increase in temperature from 37 °C, for a continuous sonication of 2 min. Similarly, Fig. 6 shows the temperature profile in a composite tissue–bone structure under these same conditions.

6 Discussion

The attenuation and subsequent regional heating of unfocused, stationary ultrasound in a composite body of tissue and bone is highly variable and more pronounced in adjacent areas with distinct material acoustic properties. It is

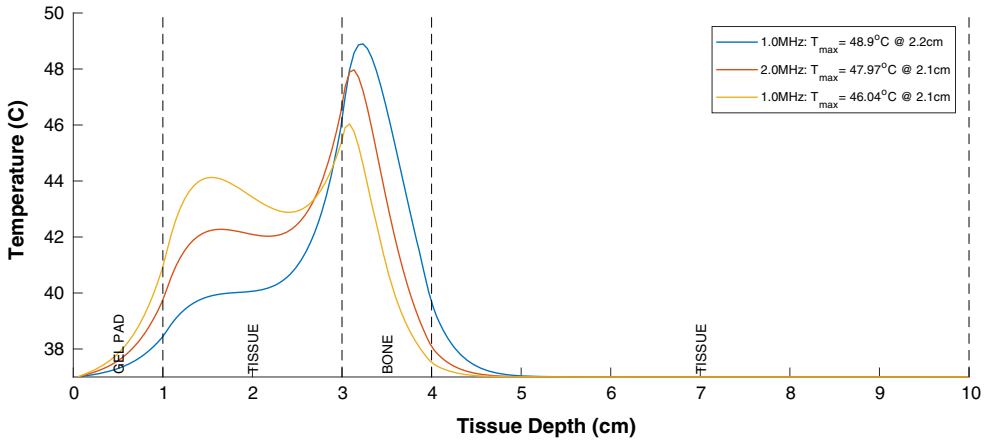

Fig. 6 Simulations showing the stationary, unfocused ultrasound heating at the interface of human soft tissue and bone at the end of a 2 min sonication of $I_{SPTA} = 1.0$ W/cm^2 at various frequencies. The maximum tissue temperature (in the bone) is shown along with the depth beyond the interface of gel pad and tissue at which it occurs

well known that at lower therapeutic utlrasound frequencies (e.g., 1 MHz), less energy is absorbed per unit volume and penetration depth is greater. This behavior is seen in the present model where there are steep differences in the energy deposited at shallow depths between 1 and 3 MHz. To benchmark the results of this sample simulation, we compare to earlier work from Marmor et al. (1979), showing the excessive heating of melanoma tumors near the scalp under up to 30 min of sonications of 0.5–1.2 W/cm^2 at 1 MHz (e.g., see Marmor et al. 1979, Fig. 5a), where interface tissues can reach 42–45 °C in a couple of minutes. Similarly, Lin et al. (2000) show high increases in simulated temperature (using the bioheat equation, including blood perfusion) at the tissue–bone interface with normal-incident ultrasound at similar input intensities and frequencies. The present model predicts between 44–47 °C interface temperatures at 2 min, depending on input frequency (see Fig. 6).

7 Summary

In summary, unfocused ultrasound primarily consist of a series of plane (longitudinal) waves which pass through all tissues within the beam profile, along the direction of wave propagation and attenuate as longitudinal and transverse waves. The energy of the waves dissipates with tissue depth via molecular friction (and subsequent heating) as well as loss to the surroundings. As the waves encounter regions with large differences in acoustic impedance (say bones), reflections, absorption and scattering occur which give rise to regional spikes in energy deposition, subsequent heating and additional loss. Presented is a relatively simple computational framework to analyze low-intensity, unfocused and stationary ultrasound-induced diathermy. As these conditions can produce undesired temperature increases at the interfaces of adjacent tissues within the body, particularly at the interface of soft tissue and bone, this framework was designed to provide an upper bound of the temperature profile within a multiphase field composed of: (1) an acoustic standoff (water-composed gel pad), (2) human soft tissue and (3) bone. The analysis was broken into three components, which were combined together to form a model of the acoustically induced heating of biotissue: (a) acoustically-induced transmission through layers of biotissue, (b) numerical 'trapping' of reflected acoustical energy at material interfaces and (c) a one-dimensional thermodynamic analysis based on the First Law, with experimentally determined acoustical power-to-heat conversion coefficients. Simulations were undertaken using a finite-difference scheme to solve the system of equations for each layer of material, providing a relatively straightforward approach without resorting to large-scale numerical simulations.

References

Arkin H, Xu LX, Holmes KR (1994) Recent developments in modeling heat transfer in blood perfused tissues. IEEE Trans Biomed Eng 41(2):97–107

Bellew James W, Michlovitz Susan L, Nolan Thomas P Jr (2016) Michlovitz's modalities for therapeutic intervention. FA Davis, Philadelphia

Betts GD et al (2000) Inactivation of food-borne microrganisms using power ultrasound in encyclopedia of food microbiology. Academic Press, Cambridge

Borejko P, Chen CF, Pao YH (2011) Application of the method of generalized rays to acoustic waves in a liquid wedge over elastic bottom. J Comput Acoust 9:41–68

Chan Andrew K et al (1973) Calculation by the method of finite differences of the temperature distribution in layered tissues. IEEE Trans Biomed Eng 2:86–90

Chan Andrew K, Sigelmann Rubens A, Guy Arthur W (1974) Calculations of therapeutic heat generated by ultrasound in fat-muscle-bone layers. IEEE Trans Biomed Eng 4:280–284

Chato JC (1990) Fundamentals of bioheat transfer. Thermal dosimetry and treatment planning. Springer, Berlin, pp 1–56

Corry Peter M et al (1982) Ultrasound-induced hyperthermia for the treatment of human superficial tumors. Int J Radiat Oncol Biol Phys 8(7):1225–1229

Dewhirst Mark W et al (2005) Re-setting the biologic rationale for thermal therapy. Int J Hyperth 21(8):779–790

Draper David O, Chris Castel J, Castel Dawn (1995) Rate of temperature increase in human muscle during 1 MHz and 3 MHz continuous ultrasound. J Orthop Sports Phys Ther 22(4):142–150

Duck Francis A (2013) Physical properties of tissues: a comprehensive reference book. Academic press, Cambridge

Elmore WC, Heald MA (1985) Physics of waves. Dover Publishers, Mineola

Fessenden P et al. (1984) Experience with a multi-transducer ultrasound system for localized hyperthermia of deep tissues (Abstract). In: 4th International symposium hyperthermic oncology, Aarhus

Frizzell Leon A, Carstensen Edwin L, Dyro Joseph F (1976) Shear properties of mammalian tissues at low megahertz frequencies. The J Acoust Soc Am 60(6):1409–1411

Fujii Mamiko et al (1999) Study of the cause of the temperature rise at the muscle-bone interface during ultrasound hyperthermia. IEEE Trans Biomed Eng 46(5):494–504

Haken Beth Ann, Frizzell LA, Carstensen EL (1992) Effect of mode conversion on ultrasonic heating at tissue interfaces. J Ultrasound in Med 11(8):393–405

Herman Bruce A, Harris Gerald R (2002) Models and regulatory considerations for transient temperature rise during diagnostic ultrasound pulses. Ultrasound in Med Biol 28(9):1217–1224

Hill Christopher Rowland, Bamber Jeff C, ter Haar Gail R (eds) (2004) Physical principles of medical ultrasonics, 2707–2707

Hynynen K, DeYoung D (1988) Temperature elevation at muscle-bone interface during scanned, focused ultrasound hyperthermia. Int J Hyperth 4(3):267–279

Hynynen K (1990) Biophysics and technology of ultrasound hyperthermia. Methods of external hyperthermic heating. Springer, Berlin, pp 61–115

King RL et al (2011) Development and characterization of a tissue-mimicking material for high-intensity focused ultrasound. In: IEEE transactions on ultrasonics, ferroelectrics, and frequency control, 58(7)

Lehmann Justus F et al (1967) Heating produced by ultrasound in bone and soft tissue. Arch Phys Med Rehabilit 48(8):397–401

Lehmann Justus F, DeLateur Barbara Jane, Silverman Donald R (1966) Selective heating effects of ultrasound in human beings. Arch Phys Med Rehabilit 47(6):331

Lin WinLi et al (2000) Theoretical study of temperature elevation at muscle/bone interface during ultrasound hyperthermia. Med Phys 27(5):1131–1140

Marmor Jane B et al (1979) Treatment of superficial human neoplasms by local hyperthermia induced by ultrasound. Cancer 43(1):188–197

Nahirnyak Volodymyr, Douglas Mast T, Holland Christy K (2007) Ultrasound-induced thermal elevation in clotted blood and cranial bone. Ultrasound in Med Biol 33(8):1285–1295

Mayer WG (1965) Energy partition of ultrasonic waves at flat boundaries. Ultrasonics 3(2):62–68

Morris Hugh et al (2008) Investigation of the viscous heating artefact arising from the use of thermocouples in a focused ultrasound field. Phys Med Biol 53(17):4759

Nell Diane M, Myers Matthew R (2010) Thermal effects generated by high-intensity focused ultrasound beams at normal incidence to a bone surface. The J Acoust Soc Am 127(1):549–559

Nelson PA, Herrick JF, Krusen FH (1950) Temperatures produced in bone marrow, bone and adjacent tissues by ultrasonic diathermy; an experimental study. Arch Phys Med Rehabilit 31(11):687

Nyborg Wesley L (2001) Biological effects of ultrasound: development of safety guidelines. Part II: general review. Ultrasound in Med Biol 27(3):301–333

Nyborg Wesley L (1988) Solutions of the bio-heat transfer equation. Phys Med Biol 33(7):785

Pennes Harry H (1948) Analysis of tissue and arterial blood temperatures in the resting human forearm. J Appl Physiol 1(2):93–122

Rhoon Van, Gerard C et al (2013) CEM43C thermal dose thresholds: a potential guide for magnetic resonance radiofrequency exposure levels? Eur Radiol 23(8):2215–2227

Shimm David S et al (1988) Scanned focussed ultrasound hyperthermia: initial clinical results. Int J Radiat Oncol Biol Phys 15(5):1203–1208

Smith Nadine Barrie et al (2001) Thermal effects of focused ultrasound energy on bone tissue. Ultrasound in Med Biol 27(10):1427–1433

Tai Bruce L et al (2015) Numerical evaluation of sequential bone drilling strategies based on thermal damage. Med Eng Phys 37(9):855–861

Virovlyanskii AL (1995) Interrelation between ray and mode field representations in an acoustic waveguide. Radiophys Quantum Electron 38(1):76–80

Wu Junru, Gonghuan Du (1990) Temperature elevation generated by a focused Gaussian beam of ultrasound. Ultrasound in Med Biol 16(5):489–498

Yarmolenko Pavel S et al (2011) Thresholds for thermal damage to normal tissues: an update. Int J Hyperth 27(4):320–343

Zohdi TI (2014) Modeling electrical power absorption and thermally-induced biological tissue damage. Biomech Model Mechanobiol 13:115–121

Zohdi TI (2007) P-wave induced energy and damage distribution in agglomerated granules. Model Simul Mater Sci Eng 15:S435–S448

Zohdi TI (2016) A discrete element and ray framework for rapid simulation of acoustical dispersion of microscale particulate agglomerations. Comput Mech 57(3):465–482